Bachelorarbeit
Zur Erlangung des akademischen Grades Bachelor of Science

Ab-Initio Investigation of Mechanical Stability and Phase Transitions of Scandium Nitride

eingereicht von: Gerome Speth

Gutachter/innen: PD Pasquale Pavone
Prof. Claudia Draxl

Eingereicht am Institut für Physik der Humboldt-Universität zu Berlin am:

Abstract

We present ab-initio calculations of the mechanical stability and phase transition of the cubic phases of scandium nitride. The computations are performed by utilizing density-functional theory, which is implemented within the **exciting** code. We used **PBE** and **PBEsol** functionals. Additionally, the pre- and post-processing tasks for elastic properties are carried out using the software tool **ElaStic**. We calculated the structural properties, investigated the phases transitions, and finally investigated the stability under deformation by calculating the elastic constants. We found small differences in the results of **PBE** and **PBEsol** and found a good agreement with the theoretical and experimental data available in the literature.

Contents

Introduction

Scandium Nitride (ScN) has emerged as a significant material in the field of semiconductor research and development, owing to its unique properties and potential applications across a wide range of cutting-edge technologies. At zero temperature and without other external perturbations, ScN crystallizes in the rocksalt crystal structure. This phase has a high melting temperature and the capacity to be doped with both n-type and p-type carriers. For these reasons, rocksalt ScN represents a promising platform for the advancement of electronic and photoelectronic device technologies. Furthermore, its versatile properties render it suitable for use in various applications, including solid-state lighting, photodetectors, sensors, high-speed power-electronic devices, and thermoelectric systems. Research on ScN not only addresses contemporary challenges in energy-efficient electronics and computing but also paves the way for innovative advancements in device functionalities and materials engineering [1].

Despite the prevalent understanding of its rocksalt structure [1] under typical conditions, it is also relevant to assess the possibility of alternative structures under varied conditions, such as changes in pressure. Exploring the mechanical stability of ScN offers an opportunity to investigate its additional properties under specific conditions. This research holds the potential to unveil novel applications through mechanical manipulation, thereby further broadening the scope of ScN's technological relevance and impact.

In our theoretical exploration, we focus on three specific cubic phases of the material: the rocksalt (`B1`), caesium-chloride (`B2`), and zincblende (`B3`) structures. Our *ab-initio* investigation proceeds in three distinct steps. Initially, we delve into the analysis of ScN's energetic properties to get insights into its structures. Additionally, we explore the presence of possible phase transitions between these structures. Finally, we investigate the elastic constants of these phases, evaluating their stability under mechanical manipulation.

The theoretical methodology used for these investigations is based on density-functional theory. All calculations presented here are performed employing the **`exciting`** software package [2] and the **`ElaStic`** toolkit [3].

Chapter 1

Theoretical Background

The general systems which are studied in this work consist of "atoms" disposed in periodic configurations. These systems are denominated crystals. In order to deal with the issue of phase stability, the main target quantity which has to be provided is the "energy" of a given phase. Due to the microscopic nature of the crystal constituents, nuclei and electrons, the correct approach to the theoretical description of crystals is quantum mechanics. Consequently, the "energies" that are playing a role for the goals of this work must be calculated quantum mechanically. A short description of the relevant part of quantum mechanics which allows for the calculation of the energy of a crystal, is given in Section 1.1. Then, for discussing the stability of different crystal phases of materials with the same atomic constituents, the relevant thermo-dynamical quantities are introduced in Section 1.2. Finally, we present in Section 1.3 some basic concepts of elasticity which are needed to study the mechanical stability of a crystal under deformations.

1.1 Basic quantum mechanics for a crystal

The quantum-mechanical description of a crystal requires the solution of the many-body Schrödinger equation for both electrons and nuclei:

$$\hat{H}_{(\mathrm{e+n})}\,\Psi(r,R) = E_{(\mathrm{e+n})}\,\Psi(r,R)\,, \tag{1.1.1}$$

where we define $r = \{\boldsymbol{r}_1, \boldsymbol{r}_2, \boldsymbol{r}_3, ..., \boldsymbol{r}_n, \}$ as the set the coordinates of all electrons and $R = \{\boldsymbol{R}_1, \boldsymbol{R}_2, \boldsymbol{R}_3, ..., \boldsymbol{R}_m, \}$ as the configuration of the nuclei. In Eq. 1.1.1, $\hat{H}_{(\mathrm{e+n})}$ is the full hamiltonian of the system, $\Psi(r,R)$ is the corresponding wave function, and $E_{(\mathrm{e+n})}$ is the full energy of electrons and nuclei. Due to the much bigger nuclear mass than the electronic one, one can use the Born-Oppenheimer approximation to separate the full wave function in an electronic and a nuclear

contribution [4]:

$$\Psi(r, R) = \psi_{\text{el}}(r, R)\, \chi_{\text{nuc}}(R)\ . \tag{1.1.2}$$

By considering a fixed (periodic) nuclear configuration, we obtain the many-electron Schrödinger equation:

$$\left[-\frac{\hbar^2}{2m} \sum_i^N \nabla_i^2 + \sum_i^N v_{\text{el-nuc}}(\boldsymbol{r}_i) + \sum_i^N \sum_{j<i} w(\boldsymbol{r}_i, \boldsymbol{r}_j) + E_{\text{nuc-nuc}}(R) \right] \psi_{\text{el}}(r, R) = E_{\text{tot}}(R)\, \psi_{\text{el}}(r, R)\ , \tag{1.1.3}$$

where $v_{\text{el-nuc}}(\boldsymbol{r})$ is the interaction potential between one electron at $\boldsymbol{r}$ and all the nuclei in the crystal, this potential will be denoted in the next as $v_{\text{ext}}(\boldsymbol{r})$; $w(\boldsymbol{r}, \boldsymbol{r}')$ is the Coulomb electron-electron interaction potential; $E_{\text{nuc-nuc}}(R)$ is the Coulomb interaction energy among all the nuclei*; and $E_{\text{tot}}(R)$ is the "total energy" of the system at the (fixed) nuclear configuration R. In this work, we do not consider electronic excitations, therefore, in the next we will focus only on the electronic ground state (GS). From now on

$$E_{\text{tot}}(R) = E_{\text{GS}}(R) \equiv E_{\text{GS}}\ . \tag{1.1.4}$$

In the last step of Eq. 1.1.4 we consider implicit the dependence on R.

The many-body problem given in Eq. 1.1.3 is too complex to be solved with reasonable resources for the number of electrons in a solid. We must find a simplification of the problem. As we are just interested in the ground state, the density-functional theory described in the next section is the best methodology.

1.1.1 Density-functional theory

The density-functional theory (DFT) is based on moving the main quantum-mechanical descriptor from the total wave function to the ground-state (GS) electron density, $n_{\text{GS}}(\boldsymbol{r})$. This move is achieved on the basis of the Hohenberg–Kohn (HK) theorems. The first HK theorem states that the external potential to the electron system (and so, the total electronic hamiltonian, too) is uniquely linked to the GS electron density [5]. This also means that all properties of the system are "functionals" of n_{GS}. In particular this is valid for the GS energy E_{GS}:

$$E_{\text{GS}}[n_{\text{GS}}] = T_0[n_{\text{GS}}] + E_{\text{ext}}[n_{\text{GS}}] + E_{\text{H}}[n_{\text{GS}}] + E_{\text{XC}}[n_{\text{GS}}]\ , \tag{1.1.5}$$

*This energy is a constant, if the nuclear configuration is fixed.

where T_0 is the kinetic-energy functional for a non-interacting electron system, E_{ext} is the external energy resulting from the interaction with and among the nuclei, E_{H} is the classical Hartree energy, and E_{XC} is the exchange-correlation (XC) energy functional, which includes all interactions between electrons which are not considered in E_{H}[†]. This XC energy functional is unknown. The second HK theorem states that the GS energy functional minimizes at the true GS electron density. Thus, this last density can be obtained by the solution of the minimization equation:

$$\frac{\delta T_0[n]}{\delta n(\boldsymbol{r})} + v_{\text{KS}}(\boldsymbol{r}, [n]) = \mu \,, \tag{1.1.6}$$

with the (electronic) chemical potential μ and the effective Kohn-Sham potential:

$$v_{\text{KS}}(\boldsymbol{r}, [n]) = v_{\text{ext}}(\boldsymbol{r}) + \frac{\delta E_H[n]}{\delta n(\boldsymbol{r})} + \frac{\delta E_{\text{XC}}[n]}{\delta n(\boldsymbol{r})} \,. \tag{1.1.7}$$

A very elegant way of formally solving the minimization equation (Eq. 1.1.6) was suggested by Kohn-Sham [6]. According to them, the GS electron-density can be written as (omitting the index GS):

$$n(\boldsymbol{r}) = \sum_i |\phi_i(\boldsymbol{r})|^2 \,, \tag{1.1.8}$$

where the single-particle wave functions, $\{\phi_i(\boldsymbol{r})\}$, are the solution of the Kohm-Sham (KS) equations:

$$h_{\text{KS}}\, \phi_i(\boldsymbol{r}) \equiv \left[-\frac{1}{2}\nabla^2 + v_{\text{KS}}(\boldsymbol{r}, [n]) \right] \phi_i(\boldsymbol{r}) = \epsilon_i\, \phi_i(\boldsymbol{r}) \,. \tag{1.1.9}$$

The last three coupled equations (Eqs. 1.1.7 to 1.1.9) must be solved self-consistently.

As the E_{ext} is given by the system and E_{H} can be calculated, the main concern is the unknown exchange-correlation energy functional, E_{XC}. For this XC functional, approximattions are needed. Some basic approximated XC functionals which are used in this work, are shortly described in the next section.

1.1.2 Exchange-correlation functionals

Exchange-correlation functionals are an essential component of DFT. Many different functionals have been introduced with different advantages and disadvantages, mostly trading accuracy for simplicity (less computational requirements) [7]. The simplest and also most used XC functionals are listed in the following.

[†]Strictly speaking E_{XC} contains also kinetic-energy contributions beyond T_0, too.

Local-density approximation

The local-density approximation (LDA) is the simplest solution for the XC energy functionals. This approximation is based on the idea of replacing locally the contributions to E_{XC} with the ones of a homogeneous electron gas with the same density of the actual system [8]. Results obtained with the LDA are surprisingly good for the total energy of simple metals, nevertheless, lattice constants and bond-lengths are strongly underestimated [8].

Generalized gradient approximation

The generalized gradient approximation (GGA) is a major advance with respect to LDA. Instead of just relying on the local value of the density, it takes also its gradient into consideration. This generally results in better approximations at a similar computational effort than LDA. Several GGA implementations are available in the literature [9]. Among them, the ones used in this work are the **`PBE`** functional, proposed by Perdew, Burke, and Ernzerhof [9], and its modification **`PBEsol`** [10]. **`PBEsol`** is designed to improve the description of solids and bulk materials. Due to an adjusted functional form, **`PBEsol`** yields more accurate lattice constants and cohesive energies [10].

1.2 Stability of a crystal structure

For isolated systems the most stable phase is the one with the lowest energy. In order to specify completely a given phase, *e.g.*, the rocksalt **`B1`** phase, it is necessary to give both the crystal symmetry of the phase and the values of the corresponding lattice parameter(s) (see Chapter 3). Then, in order to calculate the equilibrium structure corresponding to a given phase, one has first to perform calculations of the energy of the system for different values of the lattice constant(s). Secondly, the lattice parameter(s) for which the energy is minimized has (have) to be found.

Hence several energy values for different lattice parameters have been calculated, an energy-lattice function can be fitted through those values. There are many equations of state, which describe this relation. The one we use for the calculations in this work is the Birch–Murnaghan (BM) equation of state [11], mentioned in the next subsection 1.2.1. When fitted function is found, the lattice parameter corresponding the minimum of the function belongs to stable configuration of the phase(s).

1.2.1 Birch–Murnaghan equation of state

The Birch–Murnaghan (BM) equation of state [11] describes approximately the relation between energy (E) or pressure (p) of a crystal phase and the corresponding volume, V. In order to derive it, Birch started with the relation between pressure and free energy (F) at a fixed temperature T:

$$p = -\left(\frac{\partial F}{\partial V}\right)_T . \tag{1.2.1}$$

From this equation, he used an expansion around the minimum volume V_0 to get to the following expression for the pressure:

$$p(V) = \frac{3B_0}{2}\left[\left(\frac{V_0}{V}\right)^{\frac{7}{3}} - \left(\frac{V_0}{V}\right)^{\frac{5}{3}}\right]\left[1 + \frac{3}{4}(B' - 4)\left(\left(\frac{V_0}{V}\right)^{\frac{2}{3}} - 1\right)\right] , \tag{1.2.2}$$

where B_0 is the bulk modulus at equilibrium and B' the corresponding derivative with respect to the pressure. After integrating over the volume, one gets the equation for the energy dependence on the volume:

$$E(V) = E_0 + \frac{9V_0B_0}{16}\left\{\left[\left(\frac{V_0}{V}\right)^{\frac{2}{3}} - 1\right]^3 B' + \left[\left(\frac{V_0}{V}\right)^{\frac{2}{3}} - 1\right]^2\left[6 - 4\left(\frac{V_0}{V}\right)^{\frac{2}{3}}\right]\right\} , \tag{1.2.3}$$

with $E_0 = E(V_0)$.

1.2.2 Pressure-induced phase transitions

Phase transitions are changes in the structure of a material. To calculate the phase transitions in solids, we take a look at the Gibbs energy. As both phases in the transitions have the same Gibbs energy:

$$G_{\text{initial}} = G_{\text{final}} \tag{1.2.4}$$

The Gibbs energy is given by $G = E + pV - ST$. For the following calculations we use $T = 0$. Therefore the Gibbs energy (G) simplifies to a term equal the enthalpy ($H = E + pV$), hence the term $-TS$ vanishes. Resulting in the equation:

$$H_{\text{initial}} = H_{\text{final}} \tag{1.2.5}$$

or in other therms

$$E_{\text{initial}} + p_{\text{initial}}V_{\text{initial}} = E_{\text{final}} + p_{\text{final}}V_{\text{final}} \tag{1.2.6}$$

we examine solid behaviour under a certain pressure, we also consider the pressure as fixed and get a second condition:

$$p_{\text{initial}} = p_{\text{final}} \tag{1.2.7}$$

For calculating enthalpy and pressure we can use the Birch-Murnagham equation of state shown in Section 1.2.1.

1.3 Basics of elasticity

In the following section we discuss the elastic properties of solids. Every solid undergoes under relatively small "forces" an elastic deformation. When the force and with that also the correlating deformation becomes to big, the deformed material ever breaks or experiences non elastic deformation, depending an the material. For small strains these deformations obey Hooke's law.

1.3.1 Strain

For every deformation Δx we define the strain ϵ as the factor between the deformation an the original measures:

$$\Delta x = \epsilon x$$

In three dimensions ϵ becomes a three dimensional tensor:

$$\epsilon = \begin{pmatrix} \epsilon_{11} & \frac{\epsilon_{12}}{2} & \frac{\epsilon_{13}}{2} \\ \frac{\epsilon_{21}}{2} & \epsilon_{22} & \frac{\epsilon_{23}}{2} \\ \frac{\epsilon_{31}}{2} & \frac{\epsilon_{32}}{2} & \epsilon_{33} \end{pmatrix}$$

Regarding symmetric nature of the strain we get a symmetric tensor:

$$\epsilon = \begin{pmatrix} \epsilon_{11} & \frac{\epsilon_{12}}{2} & \frac{\epsilon_{13}}{2} \\ \frac{\epsilon_{12}}{2} & \epsilon_{22} & \frac{\epsilon_{23}}{2} \\ \frac{\epsilon_{12}}{2} & \frac{\epsilon_{23}}{2} & \epsilon_{33} \end{pmatrix} = \epsilon^t$$

This leads us to six independent components that can be be rearranged to a 6 dimensional vector using the so-called Voigt notation:

$$\epsilon = \begin{pmatrix} \epsilon_{11} \\ \epsilon_{22} \\ \epsilon_{33} \\ \epsilon_{23} \\ \epsilon_{13} \\ \epsilon_{12} \end{pmatrix} := \begin{pmatrix} \epsilon_1 \\ \epsilon_2 \\ \epsilon_3 \\ \epsilon_4 \\ \epsilon_5 \\ \epsilon_6 \end{pmatrix}$$

In an analog manner we can also define the stress as a 6 dimensional vector σ_j .

1.3.2 Elastic constants

By using Hooke's law we can now define the elastic constants C_{ij} as the factor between the strain ϵ and the stress σ:

$$\sigma_i = C_{ij}\epsilon_j \ ,$$

Regarding the cubic symmetry we can simplify the number of independent elastic constants. This leads us to

$$C_{11} = C_{22} = C_{33} \ ,$$

as well as

$$C_{12} = C_{13} = C_{23} \ ,$$

and

$$C_{44} = C_{55} = C_{66} \ .$$

All remaining constants vanish.

1.3.3 Stability under deformation

For examining the stability of the phases we must evaluate the Born criteria of stability. For cubic structures the stability criteria are [12]:

1. $C_{11} > |C_{12}| \ ,$
2. $C_{11} + 2C_{12} > 0 \ ,$
3. $C_{44} > 0 \ .$

Chapter 2

Computational Methodology and Parameters

In this chapter, we briefly introduce the computational tools used in this work and we give a description of the main computational parameters needed to perform the calculations. First, we present the full-potential all-electron code **exciting** [2], which we use to solve numerically the self-consistent Kohn-Sham (KS) equations (Eqs. 1.1.7 to 1.1.9) and to determine the total energy of the crystal. Then, we introduce the **ElaStic** toolkit, which is used for calculating the elastic constants.

2.1 The exciting software package

exciting is a comprehensive software package for performing first-principles electronic-structure calculations using various versions of the linearized augmented plane wave (APW) plus local orbital (LAPW+lo) method. LAPW+lo is recognized as one of the most accurate numerical approaches for solving the KS equations of DFT. One of the basic features of **exciting** is that the unit cell of the crystal is divided in two regions. The first region consists of the so-called muffin-tin (MT) spheres, centered at the position of the nuclei. Different nuclear species can have MT spheres of different radius R_{MT}. The remaining part of the unit cell is called interstitial (I) region. In the next, we focus on the basis functions used in **exciting** to expand the KS single-particle wave functions as well as the related computational parameters.

2.1.1 Basis functions

One of the main feature of **exciting** is that different functions are considered in the MT and I regions as basic functions. Inside the I region simple plane waves

are used:

$$\Phi_{\boldsymbol{k}+\boldsymbol{G}}(\boldsymbol{r}) = \frac{1}{\sqrt{\Omega}}\, \mathrm{e}^{i(\boldsymbol{k}+\boldsymbol{G})\cdot\boldsymbol{r}} \qquad \text{for } \boldsymbol{r} \in \mathrm{I}\,, \tag{2.1.1}$$

where $\boldsymbol{k}$ belongs to the first Brillouin zone of the crystal, $\boldsymbol{G}$ is a reciprocal lattice vector, and Ω is the volume of the unit cell. At variance with this, an APW basis function inside the MT sphere around the nucleus α is expressed as a combination of products of the spherical harmonic $Y_l^m(\hat{\boldsymbol{r}}_\alpha)$ and a radial function $u_l(r_\alpha)$:

$$\Phi^{\mathrm{APW}}_{\boldsymbol{k}+\boldsymbol{G}}(\boldsymbol{r}) = \sum_{lm} A_{lm}^{\boldsymbol{k}+\boldsymbol{G}}\, u_l(r_\alpha)\, Y_l^m(\hat{\boldsymbol{r}}_\alpha) \qquad \text{for } r_\alpha \leq R_{\mathrm{MT},\alpha}\,. \tag{2.1.2}$$

Here, $\boldsymbol{r}_\alpha = \boldsymbol{r} - \boldsymbol{R}_\alpha$ and A_{lm}^{k+G} are coefficients which are determined by the continuity condition for the basis functions at the boundary between the MT and I regions.

An efficient alternative to the APWs are the linearized augmented plane waves (LAPWs). In this case, the following form for the basis functions is used in the MT region:

$$\Phi^{\mathrm{APW}}_{\boldsymbol{k}+\boldsymbol{G}}(\boldsymbol{r}) = \sum_{lm} \left[A_{lm}^{\boldsymbol{k}+\boldsymbol{G}}\, u_l(r_\alpha;\varepsilon_{l\alpha}) + B_{lm}^{\boldsymbol{k}+\boldsymbol{G}}\, \dot{u}_l(r_\alpha;\varepsilon_{l\alpha})\right] Y_l^m(\hat{\boldsymbol{r}}_\alpha) \qquad \text{for } r_\alpha \leq R_{\mathrm{MT},\alpha}\,, \tag{2.1.3}$$

here, $\varepsilon_{l\alpha}$ is the so-called linearization energy, $\dot{u}_l$ is the energy derivative of u_l, and the coefficients $B_{lm}^{\boldsymbol{k}+\boldsymbol{G}}$ can be derived by imposing the continuity of the first derivative of the basis functions, too.

In addition to APWs and LAPWs, **exciting** use as further basis functions the so-called local orbitals (LOs). The LOs are non-vanishing only in the MT region and are used to improve the accuracy of the calculations.

Limitations of the number of basis functions

In order to perform an explicit calculation, the number of basis functions (APWs / LAPWs and LOs) used in the expansion of the KS single-particle wave functions must be limited to a finite value. In **exciting** this is done by fixing the value of the parameter given by the product of $R_{\mathrm{MT,min}}$, the smallest muffin-tin radius in the system, and $|\boldsymbol{k}+\boldsymbol{G}|_{\max}$, the maximum length of the vector of $\boldsymbol{k}+\boldsymbol{G}$. Choosing an appropriate value for this parameter is crucial as it balances computational resources with the need for accurate representation of the electronic states. In the next part of this work, we use the notation in which this parameter is denoted as **rgkmax**, as used in the "Input Reference" list of the **exciting** code [13]. The number of LOs used in the calculations can be changed by modifying the corresponding section in the "species files" which characterize each elemental atomic constituent [14].

Further computational parameters: $\boldsymbol{k}$-points grids, smearing coefficient

The explicit calculation of the total energy in KS-DFT codes (according to Eq. 1.1.5) requires to perform integration in reciprocal space of functions which are expensive to be evaluated on very (actually infinitely) dense $\boldsymbol{k}$-points grids. In order to keep feasible the computational effort, the integrals are approximated by sums of contributions evaluated for discrete $\boldsymbol{k}$-points grids.

In **exciting** these grids are determined by assigning three integer numbers to the parameter **ngridk** [13]. These integers represent the number of mesh points along the direction of the basis vectors in reciprocal space. Of course, the choice of **ngridk** influences the accuracy and computational efficiency of the calculations. More grid points typically lead to more accurate results but require increased computational resources.

Furthermore, attention must be paid when performing calculations for metallic systems with course $\boldsymbol{k}$-points grids. In order to determine a correct value of the Fermi energy of these systems, one has to include a smearing coefficient (called **swidth** in **exciting** [13]), for a smooth approximation to the Dirac delta functions which are required by this calculation. For finer grids the size of the parameter **swidth** should be reduced, being zero in the limit of an infinitely dense $\boldsymbol{k}$-points grid.

2.2 The ElaStic tool

The calculations of the elastic constants presented in this work are performed with the help of the **ElaStic** toolkit [3]. A graphical representation of the workflow employed by **ElaStic** is shown in Figure 2.1. **ElaStic** first determines the number of independent components of the elastic tensor for the structural symmetry of the considered crystal. To achieve this, the tool employs the program **sgroup** [15] to ascertain the space group of the crystal. according to the crystal symmetry, for all determined distortion types a set of deformed structures is created within a range of Lagrangian strains, $[-\eta_{\max}, \eta_{\max}]$. Then total-energy calculations are performed with **exciting** for each of these deformed structures. Next, energy derivatives are calculated by **ElaStic** employing polynomial fitting procedures. The energy derivatives can be expressed analytically as linear combination of the elastic constants of the considered crystal. This yields a linear system where the elastic constants are the unknown. Through solving the linear system, **ElaStic** provides the values of the second-order elastic constants, C_{ij}.

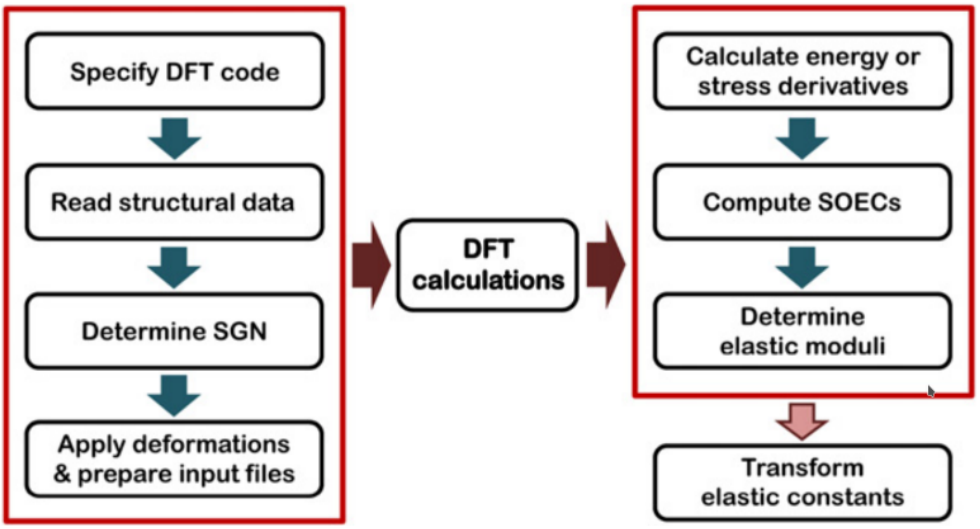

Figure 2.1: Flowchart of the algorithm used in the `ElaStic` tool (from Ref. [3]).

Chapter 3

Structure of the ScN Phases

The three phases of ScN which are investigated in this work are: The rocksalt type structure (`B1`), the CsCl type structure (`B2`), and the zincblende type structure (`B3`). All of these structures are cubic.

3.1 Phase `B1`: Rocksalt

The rocksalt structure is shown in Figure 3.1. It is a face-centered cubic structure with lattice constant a and basis vectors

$$\boldsymbol{a}_1 = \frac{a}{2}\begin{pmatrix}1\\0\\1\end{pmatrix}, \qquad \boldsymbol{a}_2 = \frac{a}{2}\begin{pmatrix}1\\1\\0\end{pmatrix}, \qquad \boldsymbol{a}_3 = \frac{a}{2}\begin{pmatrix}0\\1\\1\end{pmatrix}.$$

The atoms in unit cell are at the following positions in crystal coordinates:

$$\boldsymbol{r}_{\mathrm{Sc}} = \left(0\,,\,0\,,\,0\right), \qquad \boldsymbol{r}_{\mathrm{N}} = \tfrac{1}{2}\left(1,\,1,\,1\right).$$

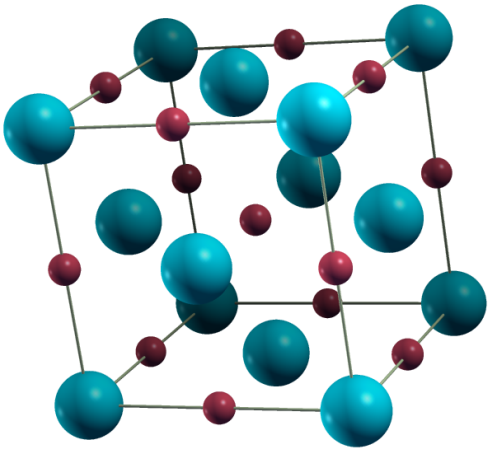

Figure 3.1: `B1` structure. Sc (N) atoms are indicated by turquoise (dark red) balls.

3.2 Phase B2:: Caesium chloride

The CsCl structure is shown in Figure 3.2. It is a primitive cubic structure with lattice constant a and basis vectors as follows

$$\boldsymbol{a}_1 = a \begin{pmatrix} 1 \\ 0 \\ 0 \end{pmatrix}, \qquad \boldsymbol{a}_2 = a \begin{pmatrix} 0 \\ 1 \\ 0 \end{pmatrix}, \qquad \boldsymbol{a}_3 = a \begin{pmatrix} 0 \\ 0 \\ 1 \end{pmatrix} .$$

The atoms in unit cell are at the following positions in crystal coordinates:

$$\boldsymbol{r}_{\mathrm{Sc}} = \left(0\,,\,0\,,\,0\right) , \qquad \boldsymbol{r}_{\mathrm{N}} = \tfrac{1}{2}\left(1,\,1,\,1\right) .$$

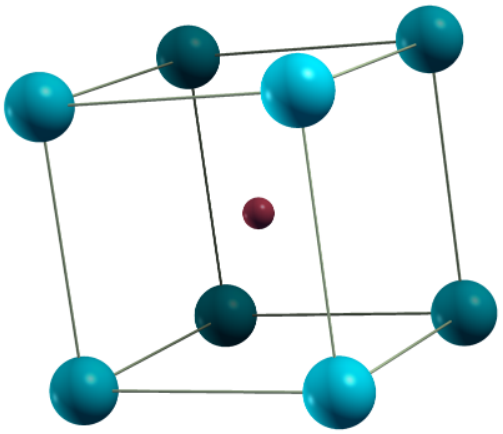

Figure 3.2: B2 structure. Sc (N) are indicated by turquoise (dark red) balls.

3.3 Phase B3: Zincblende

The zincblende structure is shown in Figure 3.3. It is a face-centered cubic structure with with lattice constant a and basis vectors as follows

$$\boldsymbol{a}_1 = \frac{a}{2}\begin{pmatrix} 1 \\ 0 \\ 1 \end{pmatrix}, \qquad \boldsymbol{a}_2 = \frac{a}{2}\begin{pmatrix} 1 \\ 1 \\ 0 \end{pmatrix}, \qquad \boldsymbol{a}_3 = \frac{a}{2}\begin{pmatrix} 0 \\ 1 \\ 1 \end{pmatrix}.$$

The atoms in unit cell are at the following positions in crystal coordinates:

$$\boldsymbol{r}_{\mathrm{Sc}} = \big(0\,,\,0\,,\,0\big)\,, \qquad \boldsymbol{r}_{\mathrm{N}} = \tfrac{1}{4}\big(1,\,1,\,1\big)\,.$$

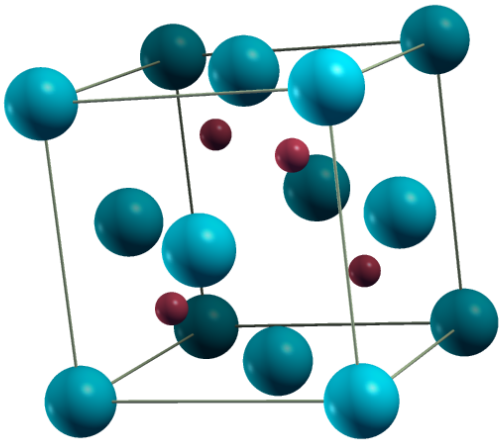

Figure 3.3: B3 structure. Sc (N) atoms are indicated by turquoise (dark red) balls.

Chapter 4

Results and Discussion

In this chapter, we present the outcomes of our computational investigations on the structural properties of the phases. As we try to improve the accuracy, we reach convergence in our given from for all properties. We use methodology of **PBE** and **PBEsol** separately and reach convergence for different values in both. In comparison with other calculations and experiments we try to solve the question of the adequate method for our investigation.

4.1 Equilibrium structural properties

For each structure type tests were made to determine the optimal constant of the unit cell. These test were repeated for different values of **ngridk** and **rgkmax**. The results reached convergence for the higher values. For the **rgkmax** the starting value was 7 for each iteration and the highest value was 9. In the following we can see the convergence behaviour for the values at the zero pressure point of the energy E_0, volume V_0, the Bulk modulus B_0 the derivative of the bulk modulus B' and the lattice constant a_0, all shown in Tables A.1 to A.6 in the appendix.

We settle for the converged parameters as stated in the Table 4.1 for **PBEsol** and Table 4.2 for **PBE**. For better comparison with other studies, we show the values of the lattice parameters in units of both Bohr and Å.

Table 4.1: Converged structural parameters using **PBEsol**.

Phase	E_0 [Ha]	V_0 [Bohr^3]	V_0 [Å^3]	a_0 [Bohr]	a_0 [Å]	B_0 [GPa]	B'
B1	-818.044	150.462	22.296	8.4430	4.4678	212.0	4.12
B2	-817.969	140.872	20.875	5.2032	2.7534	194.7	4.11
B3	-818.016	191.611	28.394	9.1515	4.8428	148.5	3.88

.

Table 4.2: Converged structural parameters using **PBE**.

Phase	E_0 [Ha]	V_0 [Bohr^3]	V_0 [Å^3]	a_0 [Bohr]	a_0 [Å]	B_0 [GPa]	B'
B1	-819.132	155.109	22.985	8.5290	4.5134	197.9	4.08
B2	-819.056	146.003	21.635	5.2656	2.7864	179.6	4.12
B3	-819.110	197.217	29.225	9.2399	4.8895	140.0	3.85

.

4.1.1 Comparison with literature values

Upon reviewing the calculated lattice constants in comparison to previous studies (see Table 4.3), we find our results consistent to other values in the literature. As most theoretical values in the literature are obtained using the **PBE** functional, they (mostly) align with our calculation. Also the experimental value for the **B1** phase is consistent with our **PBE** calculation. Even so there is just one experimental value, this still serves as a useful benchmark for our calculations. Over all we receive slightly lower lattice constants from the **PBEsol**.

When we compare the ab-initio publications regarding the bulk modulus B_0 and its derivative B' showcase proximity to our **PBE** calculations, while the **PBEsol** overestimates. The experimental data is consistent with both of our calculations.

Table 4.3: Comparing literature for the structural properties.

Phase		E_{XC}	Ref.	a_0 [Å]	B_0 [GPa]	B'
B1	This work	**PBEsol**		4.4678	212.02	4.12
	This work	**PBE**		4.5134	197.90	4.08
	Experiment		[16]	4.519±0.005	182.7±40	
	FP-LAPW	**LDA**	[17]	4.435	220	3.45
	PW	**PBE**	[18]	4.51	202.0	3.70
	FP-LAPW	**PBE**	[19]	4.516	196.958	3.78
	FP-LAPW	**PBE**	[20]	4.54	201	3.31
	FPLMTO	**PBE**	[21]	4.651	210.364	3.1225
	FP-LAPW	**PBE**	[22]	4.520	201.576	3.89
	FP-LAPW	**PBE**	[23]	4.5197	201.12	4.24
	PW	**PBE**	[24]	4.57	174.75	
B2	This work	**PBEsol**		2.7534	194.71	4.11
	This work	**PBE**		2.7864	179.57	4.12
	FP-LAPW	**LDA**	[17]	2.961	180	4.15
	PW	**PBE**	[18]	2.79	179.5	3.80
	FP-LAPW	**PBE**	[19]	2.789	176.163	3.991
	FP-LAPW	**PBE**	[20]	2.81	170	3.47
	FPLMTO	**PBE**	[21]	2.926	159.759	3.0335
	FP-LAPW	**PBE**	[22]	2.79	178.60	4.43
	FP-LAPW	**PBE**	[23]	2.787	183.67	5.24
	PW	**PBE**	[24]	2.82	155.17	
B3	This work	**PBEsol**		4.8428	148.47	3.88
	This work	**PBE**		4.8895	139.97	3.85
	FP-LAPW	**PBE**	[19]	4.892	137.692	3.756
	FP-LAPW	**PBE**	[20]	4.88	153	3.34
	FPLMTO	**PBE**	[21]	4.939	145.195	3.433
	FP-LAPW	**PBE**	[23]	4.989	143.25	4.37
	PW	**PBE**	[24]	4.96	122.66	
	pseudo potential	**PBE**	[25]	4.8875	142.06	3.6946
	pseudo potential	**LDA**	[25]	4.8001	159.42	3.7087
	pseudo potential	**PBEsol**	[25]	4.911	142.68	3.942

4.2 Relative phase stability under pressure

For calculating the energy values, we use the values calculated in a broader volume range than in the convergence tests before, but using the computational parameter established in these tests. The results of the calculations for the energy in dependence of the volume are fitted again using the Birch-Murnaghan equation of state. The parameters of the equation of state obtained by the fit deviates slightly from those reported in the previous sections, due to the larger volume range. The results are shown in Figure 4.1. Regarding the three phases, we can easily see that the `B1` structure shows the lowest energy minimum of all the configurations. Therefore, it is the most stable phase at zero pressure. At smaller value of the volume per unit cell, the `B2` phase has a lower energetic value than the `B1` one. A transition between both phases is therefore possible by imposing an external pressure. The `B3` phase occupies lower energy values at high lattice constant. For reaching this the stable environment of this state, a negative pressure must be applied.

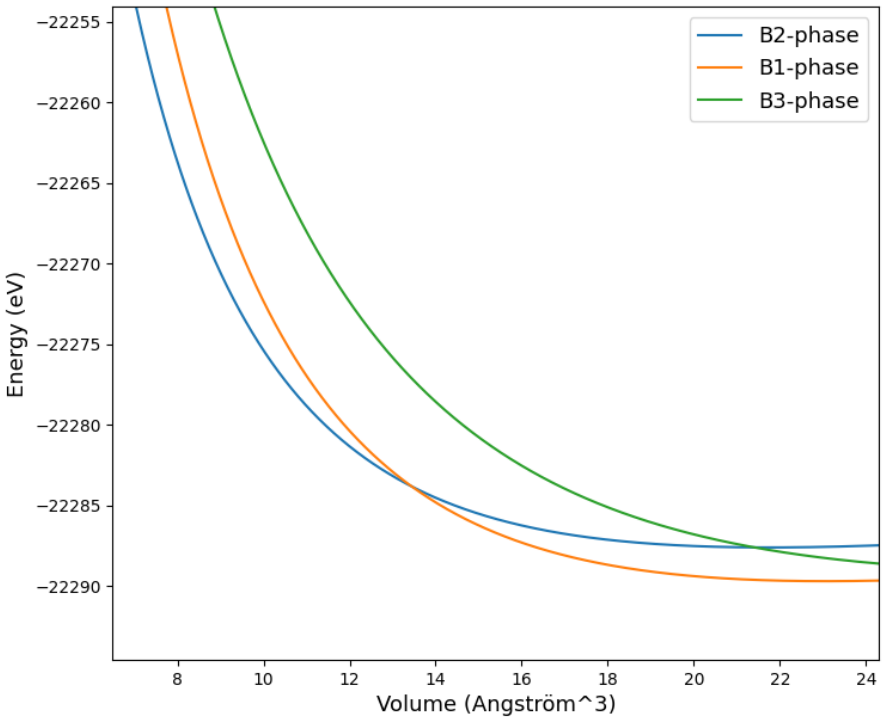

Figure 4.1: The three cubic phases of ScN.

4.2.1 `B1-B2` phase transition

The transition from the **`B1`** phase to the **`B2`** phase represents is the only physically real transition found. In the **`PBEsol`** simulation, this transition occurs between a volume of 12.8 Å^3 for the **`B2`** phase and 13.9 Å^3 for the **`B1`** phase, corresponding to a pressure of 253.5 GPa (compare Figure 4.2). At this transition point, the enthalpy reaches 22233.6 eV.

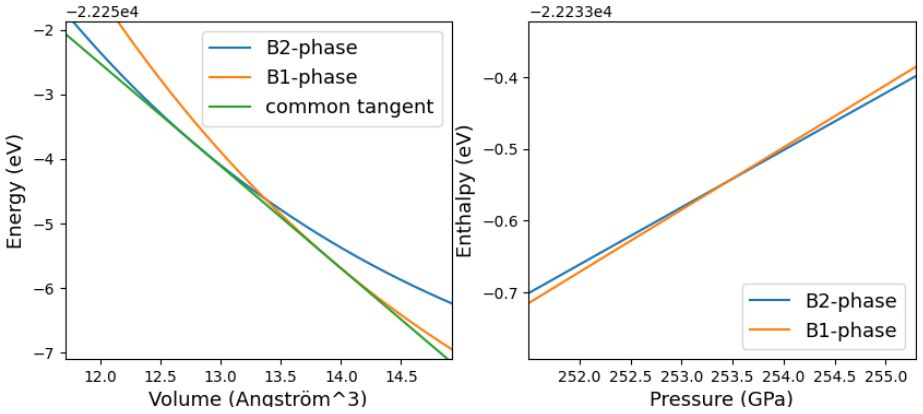

Figure 4.2: Phase transition using **`PBEsol`**.

The **`PBE`** simulation leads to really similar volume. Here, this transition occurs between a volume of 12.8 Å^3 for the **`B2`** phase and 14.0 Å^3 for the **`B1`** phase, but corresponding to a pressure is 262 GPa (see Figure 4.3). At this transition point, the enthalpy reaches −22261.9 eV.

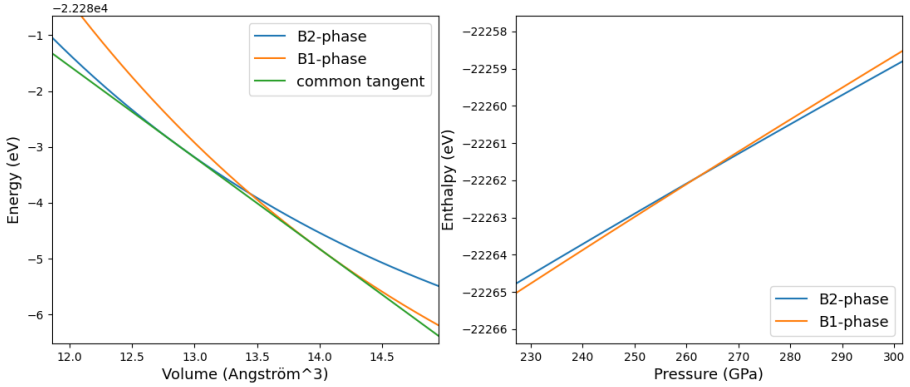

Figure 4.3: Phase transition using **`PBE`**.

4.2.2 B2-B3 phase transition

The phase transition between B2 and B3 is overshadowed by the phase transition of B1-B2.

4.2.3 B1-B3 phase transition

Theoretical transitions between the B1 and B3 exists. This transition at high pressure is not physically realised because it is overshadowed by the B1-B2 phase transitions. There is also a transition at negative pressure, but the physical practicality of this condition condemns this transition to a theoretical play.

4.3 Stability under mechanical manipulation

To determine the stability of the phases, looking at the total energy is not enough. Another indicator of stability are the elastic constants. In a first attempt of evaluate the question of stability, we regard the elastic constants at the minimum of the Birch-Murnaghan equation. These optima for the lattice constants are were determined in Section 1.3.2. The lattice constants are represented as 6×6 matrices:

$$C = \begin{pmatrix} C_{11} & C_{12} & C_{12} & & & \\ C_{12} & C_{11} & C_{12} & & & \\ C_{12} & C_{12} & C_{11} & & & \\ & & & C_{44} & & \\ & & & & C_{44} & \\ & & & & & C_{44} \end{pmatrix}$$

4.3.1 Elastic constants at zero pressure

Using the lattice constant at zero pressure, we can now calculate the elastic constants of each phase in the energetic minimum. Hence each phase takes this state without any outside influence, we can deduces the stability of each phase from the elastic constants. We use eleven points for nearly all calculation with a maximal strain of 0.05, but for the **B2** phase. There we used a maximum strain of 0.15, because of conflict in the literature about stability of the phase (see below).

Table 4.4: Second-order elastic constants at zero pressure

Phase	E_{XC}	C_{11}	C_{12}	C_{44}
B1	**PBEsol**	424.3	106.3	171.2
	PBE	383.8	105.2	166.9
B2	**PBEsol**	552.9	16.5	-131.2
	PBE	540.7	-0.5	-128.5
B3	**PBEsol**	161.9	120.5	66.2
	PBE	171.5	124.4	70.1

At the optimized volume of the **B1** structure and the **B3** structure all three Born criteria of stability are satisfied in **PBE** and **PBEsol**. These structures can be considered stable in reference to deformation. The **B2** structure violates the third Born criteria $C_{44} > 0$ in both methods, therefor it is not a stable structure under zero pressure. But this state wouldn't be realised in nature either way, as the **B1** structure possesses a lower energy in at the minimal volume of the **B3**

structure. More important are the elastic constants of **B2** at volumes were the **B2** structure possesses lower energies than its **B1** counterpart.

4.3.2 Elastic constants under pressure

Since there is transition to the **B2** phase, its stability is of special significance beyond the transition point. To assess this stability, we computed the elastic constants at pressures near, but exceeding, the critical pressures using the **PBE** functional. After our investigation we get the results shown in Table 4.5.

Table 4.5: Comparing literature for the elastic constants.

E_{XC}	pressure	C_{11}	C_{12}	C_{44}
PBE	278 GPa	1439.7	653.2	349.3

For evaluating the stability under pressure, we must check the pressure-adjusted born criteria of stability:

1. $C_{11} - p > |C_{12} + p|$,
2. $C_{11} + 2C_{12} + p > 0$,
3. $C_{44} - p > 0$.

In the **PBE** simulation, the **B2** phase meets all stability criteria, confirming its stability under these conditions.

4.3.3 Comparison with literature values

Upon reviewing the literature of the elastic constants, shown in Table 4.6, we encounter a scarcity of publications for comparison. However, we do have four publications available for the **B1** phase. Only two use the **PBE** functional, where one is consistent with our **PBE** calculation. The other one has a significant smaller C_{11}, while the other two constants are closer to our values. For the **B3** phase there are two sources. One of them investigated the phase with three different functionals, where the **PBE** method totally aligns with our **PBE** calculation. All other values are really close to both our calculations, but deviate a bit from them. Nonetheless, the works available in the literature confirms the stability of the **B1** and **B3** phase. The two works in the literature on the **B2** phase provide contradictory results on the topic of mechanical stability [17] [24]. One supports it [17]. The other denies it [24]. As we made these calculations with a higher accuracy and

both functional methods lead to the same conclusion, there lies a great reliability in our calculation. We also did a short test run for **LDA** functional use in the publication, but this also lead to a negative C_{44}. As there is a transition in the **B2** phase from insulator to conductor close to lattice constant of zero pressure and **PBE** underestimates the band gap, there is still some debate left.

Table 4.6: Comparing literature for the elastic constants at zero pressure.

Phase		E_{XC}	Ref.	C_{11}	C_{12}	C_{44}
B1	This work	**PBEsol**		424.3	106.3	171.2
	This work	**PBE**		383.8	105.2	166.9
	FP-LAPW	**PBE**	[19]	380.9	104.56	167.18
	FP-LAPW	**LDA**	[17]	392	134	167
	EPM (no DFT)		[26]	299	128	120
	PW	**PBE**	[24]	331.85	96.20	163.85
B2	This work	**PBEsol**		552.9	16.5	-131.2
	This work	**PBE**		540.7	-0.5	-128.5
	FP-LAPW	**LDA**	[17]	295	123	148
	PW	**PBE**	[24]	571.6	-53.050	-101.60
B3	This work	**PBEsol**		161.9	120.5	66.2
	This work	**PBE**		171.5	124.4	70.1
	pseudo potential	**PBE**	[25]	171.61	124.34	70.82
	pseudo potential	**LDA**	[25]	187.59	143.15	72.22
	pseudo potential	**PBEsol**	[25]	173.42	129.69	74.7
	PW	**PBE**	[24]	153.87	107.06	68.84

Conclusions and Outlook

In this study, we delved into the mechanical stability and phase transitions of Scandium Nitride (ScN), employing ab-initio methods to calculate several key properties and parameters. Our investigations provided insights into the behavior of ScN under different conditions.

Analyzing the total energy of different phases, we confirmed the rocksalt structure as the predominant phase under pressure-free conditions, while highlighting the dominance of the `B2` phase at higher pressures. Additionally, our contribution to the understanding of ScN's structural properties surpasses that of previous ab-initio calculations, demonstrating a higher level of accuracy.

On the field of Phase transitions we have found a transition between the `B1` and the `B2` phase and have shown that the transitions of `B3` have no physical reality.

Furthermore, our analysis of elastic constants revealed the stability of the `B1` and `B3` structures under zero-pressure conditions. Although in our calculations the `B2` phase exhibits instability under zero pressure, further investigations with functionals of higher accuracy could lead to deeper understanding of the phase. As a novelty to the discourse, our findings support the stability of the `B2` phase near the transition point to the `B1` phase, showing the existence of a stable `B2` phase under high-pressure conditions.

Because our focus remained on the cubic phase of ScN, an obvious expansion of the study would be to calculate the non-cubic phases of ScN. This could unveil more stable structures under pressure and/or higher temperatures. This exploration promises to enhance our understanding of ScN's behavior and paves the way for further advancements in its application.

Appendix A

Convergence

A.1 PBEsol

Table A.1: Convergence with **PBEsol** at the minimum energy of E_0,V_0, B_0, B', and a_0 in dependence of the values of the computational parameters **ngridk** and **rgkmax** for the NaCl-type (**B1**) structure.

B1	**ngridk**	8×8×8	12×12×12	16×16×16	20×20×20
	rgkmax				
	7	-818.0426	-818.0426	-818.0426	-818.0426
E_0 [Ha]	8	-818.0435	-818.0436	-818.0436	-818.0435
	9	-818.0436	-818.0437	-818.0437	-818.0437
	7	150.443	150.499	150.499	150.498
V_0 [Bohr^3]	8	150.417	150.455	150.458	150.465
	9	150.414	150.450	150.458	150.462
	7	212.0	211.8	211.8	211.8
B_0 [GPa]	8	212.2	212.1	212.3	212.0
	9	212.2	212.2	212.0	212.0
	7	4.20	4.11	4.10	4.11
B'	8	4.19	4.14	4.10	4.12
	9	4.19	4.14	4.12	4.12
	7	8.4426	8.4437	8.4437	8.4437
a_0 [Bohr]	8	8.4421	8.4429	8.4429	8.4430
	9	8.4421	8.4428	8.4429	8.4430

Table A.2: Convergence with `PBEsol` at the minimum energy, E_0,V_0, B_0, B' and a_0 in dependence of the values of the computational parameters `ngridk` and `rgkmax` for the CsCl-type (`B2`) structure.

`B2`	`ngridk`	8×8×8	12×12×12	16×16×16	20×20×20
`rgkmax`					
	7	-817.9676	-817.9675	-817.9676	-817.9676
E_0 [Ha]	8	-817.9685	-817.9684	-817.9685	-817.9685
	9	-817.9685	-817.9687	-817.9686	-817.9686
	7	140.927	140.984	140.903	140.900
V_0 [Bohr^3]	8	140.894	140.956	140.868	140.868
	9	140.868	140.893	140.874	140.872
	7	194.7	195.1	194.7	194.8
B_0 [GPa]	8	194.6	194.7	194.6	194.7
	9	194.7	194.6	194.6	194.7
	7	4.07	4.14	4.06	4.09
B'	8	4.11	4.14	4.09	4.11
	9	4.11	4.11	4.09	4.11
	7	5.2039	5.2046	5.2036	5.2036
a_0 [Bohr]	8	5.2035	5.2043	5.2032	5.2032
	9	5.2035	5.2035	5.2033	5.2032

Table A.3: Convergence with `PBEsol` at the minimum energy, E_0,V_0, B_0, B' and a_0 in dependence of the values of the computational parameters `ngridk` and `rgkmax` for the CsCl-type (`B3`) structure.

B3	**ngridk**	8×8×8	12×12×12	16×16×16	20×20×20
	rgkmax				
	7	-818.015	-818.015	-818.015	-818.015
E_0 [Ha]	8	-818.016	-818.016	-818.016	-818.016
	9	-818.016	-818.016	-818.016	-818.016
	7	191.607	191.597	191.591	191.591
V_0 [Bohr^3]	8	191.608	191.610	191.610	191.610
	9	191.611	191.611	191.611	191.611
	7	148.6	148.6	148.6	148.5
B_0 [GPa]	8	148.5	148.5	148.5	148.5
	9	148.4	148.4	148.4	148.4
	7	3.91	3.91	3.93	3.93
B'	8	3.88	3.88	3.88	3.88
	9	3.88	3.88	3.88	3.88
	7	9.1515	9.1513	9.1512	9.1512
a_0 [Bohr]	8	9.1515	9.1515	9.1515	9.1515
	9	9.1515	9.1515	9.1515	9.1515

A.2 PBE

Table A.4: Convergence with **PBE** at the minimum energy of E_0,V_0, B_0, B', and a_0 in dependence of the values of the computational parameters **ngridk** and **rgkmax** for the NaCl-type (**B1**) structure.

B1	**ngridk**	8×8×8	12×12×12	16×16×16	20×20×20
	rgkmax				
	7	-819.131	-819.131	-819.131	-819.131
E_0 [Ha]	8	-819.132	-819.132	-819.132	-819.132
	9	-819.132	-819.132	-819.132	-819.132
	7	155.132	155.148	155.164	155.16
V_0 [Bohr^3]	8	155.090	155.102	155.113	155.114
	9	155.086	155.097	155.108	155.109
	7	196.9	197.7	197.7	197.7
B_0 [GPa]	8	197.2	197.8	197.9	197.9
	9	197.2	197.8	197.9	197.9
	7	4.14	4.08	4.06	4.07
B'	8	4.14	4.10	4.08	4.08
	9	4.14	4.10	4.08	4.08
	7	8.5294	8.5297	8.5300	8.5299
a_0 [Bohr]	8	8.5287	8.5289	8.5291	8.5291
	9	8.5286	8.5288	8.5290	8.5290

Table A.5: Convergence with **PBE** at the minimum energy, E_0,V_0, B_0, B' and a_0 in dependence of the values of the computational parameters **ngridk** and **rgkmax** for the CsCl-type (**B2**) structure.

B2	**ngridk**	8×8×8	12×12×12	16×16×16	20×20×20
rgkmax					
	7	-819.0551	-819.0550	-819.0550	-819.0550
E_0 [Ha]	8	-819.0560	-819.0559	-819.0559	-819.0559
	9	-819.0561	-819.0560	-819.0560	-819.0560
	7	146.080	146.126	146.039	146.041
V_0 [Bohr^3]	8	146.041	146.089	145.999	146.002
	9	146.044	146.092	146.003	146.000
	7	180.0	179.7	179.84	179.8
B_0 [GPa]	8	179.6	179.5	179.6	179.6
	9	179.6	179.4	179.6	179.6
	7	4.04	4.10	4.09	4.09
B'	8	4.07	4.13	4.12	4.12
	9	4.07	4.13	4.12	4.12
	7	5.2666	5.2672	5.2661	5.2661
a_0 [Bohr]	8	5.2661	5.2667	5.2656	5.2657
	9	5.2662	5.2667	5.2657	5.2656

Table A.6: Convergence with **PBE** at the minimum energy, E_0,V_0, B_0, B' and a_0 in dependence of the values of the computational parameters **ngridk** and **rgkmax** for the CsCl-type (**B3**) structure.

B3	**ngridk**	8×8×8	12×12×12	16×16×16	20×20×20
	rgkmax				
E_0 [Ha]	7	-819.1090	-819.1090	-819.1090	-819.1090
	8	-819.1100	-819.1100	-819.1100	-819.1100
	9	-819.1100	-819.1101	-819.1101	-819.1101
V_0 [Bohr^3]	7	197.208	197.215	197.213	197.217
	8	197.212	197.213	197.213	197.213
	9	197.212	197.217	197.217	197.217
B_0 [GPa]	7	139.8	139.9	139.8	139.8
	8	140.0	140.0	140.0	140.0
	9	140.0	140.0	140.0	140.0
B'	7	3.88	3.86	3.86	3.86
	8	3.85	3.85	3.85	3.85
	9	3.85	3.85	3.85	3.85
a_0 [Bohr]	7	9.2398	9.2399	9.2399	9.2399
	8	9.2398	9.2399	9.2398	9.2399
	9	9.2398	9.2399	9.2399	9.2399

List of Figures

List of Tables

Bibliography

[1] Bidesh Biswas and Bivas Saha. Development of semiconducting scn. *PHYSICAL REVIEW MATERIALS*, 3, 2019. doi: 10.1103/PhysRevMaterials.3.020301.

[2] A. Gulans, S. Kontur, C. Meisenbichler, D. Nabok, P. Pavone, S. Rigamonti, S. Sagmeister, U. Werner, and C. Draxl. exciting: a full-potential all-electron package implementing density-functional theory and many-body perturbation theory. *J. Phys.: Condens. Matter*, 26, 2014. doi: 10.1088/0953-8984/26/36/363202.

[3] Rostam Golesorkhtabar, Pasquale Pavone, Jürgen Spitaler, Peter Puschnig, and Claudia Draxl. Elastic: A tool for calculating second-order elastic constants from first principles. *Computer Physics Communications*, 184(8): 1861–1873, 2013.

[4] Oppenheimer R. Born M. Zur quantentheorie der molekeln. *ANNALEN DER PHYSIK Vierte Folge. BAND 84*, pages 457–552, 1927.

[5] P. Hohenberg and W. Kohn. Inhomogeneous electron gas. *Physical Review*, 136(3):B864, November 1964. doi: 10.1103/PhysRev.136.B864. Received 18 June 1964.

[6] Sham L. J. Kohn W. Self-consistent equations including exchange and correlation effects. *PHYSICAL REVIEW*, 140, number 4A:A1133–A1138, 1964.

[7] John P. Perdew and Karla Schmidt. Jacob's ladder of density functional approximations for the exchange-correlation energy. *AIP Conference Proceedings*, 493:1–20, 2001. doi: https://doi.org/10.1063/1.1390175.

[8] U von Barth and L Hedin. A local exchange-correlation potential for the spin polarized case. i. *Journal of Physics C: Solid State Physics*, 5(13):1629, jul 1972. doi: 10.1088/0022-3719/5/13/012. URL https://dx.doi.org/10.1088/0022-3719/5/13/012.

[9] Matthias Ernzerhof John P. Perdew, Kieron Burke. Generalized gradient approximation made simple. *Phys. Rev. Lett. 77*, pages 3865–3868, 1996.

[10] Ga´bor I. Csonka Oleg A. Vydrov Gustavo E. Scuseria Lucian A. Constantin Xiaolan Zhou 1 John P. Perdew, Adrienn Ruzsinszky and Kieron Burke. Restoring the density-gradient expansion for exchange in solids and surfaces. *PPhys. Rev. Lett. 45*, pages 136406–1 – 136406–4, 2008.

[11] Francis Birch. Finite elastic strain of cubic crystals. *Phys. Rev.*, 71:809–824, Jun 1947. doi: 10.1103/PhysRev.71.809. URL https://link.aps.org/doi/10.1103/PhysRev.71.809.

[12] Max Born and Kun Huang. *Dynamical Theory of Crystal Lattices*. Oxford University Press, Oxford, 1954.

[13] The exciting code: Input reference for exciting fluorine. http://exciting.wikidot.com/ref:input, . Accessed: 15.03.2024.

[14] Understanding the exciting species files. http://exciting.wikidot.com/neon-understanding-species, . Accessed: 15.03.2024.

[15] A.N. Timoshevskii B.Z. Yanchitsky. Determination of the space group and unit cell for a periodic solid. *Computer Physics Communications*, 139:235–242, 2001. doi: https://doi.org/10.1016/S0010-4655(01)00212-0.

[16] D. Gall, I. Petrov, P. Desjardins, and J. E. Greene. Microstructural evolution and Poisson ratio of epitaxial ScN grown on TiN(001)/MgO(001) by ultrahigh vacuum reactive magnetron sputter deposition. *Journal of Applied Physics*, 86(10):5524–5529, 11 1999. ISSN 0021-8979. doi: 10.1063/1.371555. URL https://doi.org/10.1063/1.371555.

[17] A.T. Asvini Meenaatci, R. Rajeswarapalanichamy, and K. Iyakutti. Investigation of structural stability and electronic properties of group iii nitrides: a first principles study. *Phase Transitions*, 86(6):570–584, 2013. URL https://doi.org/10.1080/01411594.2012.713486.

[18] Premlata Pandit, Bipul Rakshit, and Sankar P. Sanyal. Ab initio study of structural, electronic, elastic, and phonon properties of scn and scp at ambient and high pressure. *Journal of Applied Physics*, 108:073528, 2010. doi: 10.1063/1.3483909.

[19] Wenxia Feng, Shouxin Cui, Haiquan Hu, Guiqing Zhang, Zengtao Lv, and Zizheng Gong. Phase stability, electronic and elastic properties of

scn. *Physica B: Condensed Matter*, 405(11):2599–2603, 2010. ISSN 0921-4526. doi: https://doi.org/10.1016/j.physb.2010.03.042. URL https://www.sciencedirect.com/science/article/pii/S0921452610002942.

[20] N. Takeuchi. First-principles calculations of the ground-state properties and stability of scn. *Physical Review B*, 65:045204, 2002. doi: https://doi.org/10.1103/PhysRevB.65.045204.

[21] A. Tebboune, D. Rached, A. Benzair, N. Sekkal, and A.H. Belbachir. A. tebboune, d. rached, a. benzair, n. sekkal, a.h. belbachir, phys. status solidi (b) 243 (2006) 2788. *Physica Status Solidi (b)*, 243:2788, 2006.

[22] A. Maachou, B. Amrani, and M. Driz. A. maachou, b. amrani, m. driz, physica b 388 (2007) 384. *Physica B*, 388:384, 2007.

[23] R. Yagoub, H. Rekkab Djabri, S. Daoud, N. Beloufa, M. Belarbi, A. Haichour, C. Zegadi, and S. Louhibi Fasla. First principles study of high-pressure phases of scn. *Ukrainian Journal of Physics*, 66(8):699, 2021.

[24] Oliver Mnisi. Density functional theory study of electronic and optical properties of scn nitride in nacl-b1, cscl-b2, zb-b3 and nias-b8 phases. *Bulletin of Materials Science*, 45, 03 2022. doi: 10.1007/s12034-021-02601-4.

[25] Mohamed Amine Ghebouli, Brahim Ghebouli, Aldjia Zeghad, Tayeb Chihi, Messaoud Fatmi, and Sameh Ibrahim Ahmed. First-principles calculations to investigate structural, elastic, electronic, lattice dynamic and optical properties for scandium and yttrium nitrides in zinc blend structure. *Journal of Materials Research and Technology*, 14:1958–1968, 2021. ISSN 2238-7854. doi: https://doi.org/10.1016/j.jmrt.2021.07.073. URL https://www.sciencedirect.com/science/article/pii/S2238785421007365.

[26] Y. Oussaïfi, A.B. Fredj, M. Debbichi, N. Bouarissa, and M. Said. Y. oussaifi, a.b. fredj, m. debbichi, n. bouarissa, m. said, semicond. sci. technol. 22 (2007) 641. *Semiconductor Science and Technology*, 22:641, 2007.

Acknowledgments

I thank Sven Lubeck for providing the species files used in this thesis prior to publication. Moreover, I want to thank Pasquale Pavone for supervising and assisting me throughout the bachelor thesis process. I also want to thank my mother for her understanding and my father for his unwavering support. Finally, I want to thank Eike Eberhardt for giving advice and needed distraction.

Selbstständigkeitserklärung

Ich erkläre hiermit, dass ich die vorliegende Arbeit selbstständig verfasst und noch nicht für andere Prüfungen eingereicht habe. Sämtliche Quellen einschließlich Internetquellen, die unverändert oder abgewandelt wiedergegeben werden, insbesondere Quellen für Texte, Grafiken, Tabellen und Bilder, sind als solche kentlich gemacht. Mir ist bekannt, dass bei Verstößen gegen diese Grundsätze ein Verfahren wegen Täuschungsversuchs bzw. Täuschung eingeleitet wird.

Berlin, ...